

Nonlinear single Compton scattering of an electron wave-packet

A. Angioi, F. Mackenroth,^{*} and A. Di Piazza[†]

Max-Planck-Institut für Kernphysik, Saupfercheckweg 1, 69117 Heidelberg, Germany

(Dated: May 4, 2016)

Nonlinear single Compton scattering has been thoroughly investigated in the literature under the assumption that initially the electron has a definite momentum. Here, we study a more general initial state, and consider the electron as a wave-packet. In particular, we investigate the energy spectrum of the emitted radiation and show that in typical experimental situations some features of the spectra shown in previous works are almost completely washed out. Moreover, we show that at comparable relative uncertainties, the one in the momentum of the incoming electron has a larger impact on the photon spectra at a fixed observation direction than the one on the laser frequency.

I. INTRODUCTION

According to classical electrodynamics a charged particle (an electron, for definiteness) accelerated by a background electromagnetic field emits radiation [1]. In the underlying quantum theory, QED, the radiation process is rather described as the emission of photons by the electron [2, 3]. Due to energy-momentum conservation a free electron is stable and cannot emit photons. The scattering of an electron with a single photon is known as (linear) Compton scattering. In general, the simultaneous interaction of an electron with many photons is suppressed by the appearance in the interaction probabilities of a corresponding power of the fine-structure constant $\alpha_{QED} \approx 1/137 \ll 1$. However, if the electron interacts with a coherent collection of photons, like those in a laser beam, the effective coupling strength appearing in perturbative expansions is not just α_{QED} , but it also depends on the typical amplitude and angular frequency of the laser field [4]. Qualitatively it is clear that a laser field characterized by an amplitude \mathcal{E} and by an angular frequency ω is able to transfer

^{*} Currently at: Department of Applied Physics, Chalmers University of Technology, Gothenburg, Sweden

[†] dipiazza@mpi-hd.mpg.de

to the electron (charge $e < 0$ and mass m) a number of photons of the order of

$$\xi = \frac{|e|\mathcal{E}}{\omega mc}, \quad (1)$$

in the typical QED length $\lambda_C = \hbar/mc \approx 3.9 \times 10^{-11}$ cm (Compton wavelength) [4–6]. Thus, at $\xi \gtrsim 1$ the probability for the electron of exchanging more than one photon with the laser field is not suppressed and the laser-electron interaction has to be taken into account exactly in the calculations. From a classical point of view, the condition $\xi \gtrsim 1$ corresponds to the onset of relativistic effects in the electron dynamics, which render the latter nonlinear with respect to the laser amplitude. Now, if the electron enters a plane-wave field with a four-momentum $p^\mu = (\varepsilon/c, \mathbf{p})$, with $\varepsilon = (m^2 c^4 + |\mathbf{p}|^2 c^2)^{1/2}$, and in the process of photon emission it absorbs ξ laser photons, due to the Doppler effect, the typical energy $\hbar\omega'$ of the emitted photon is of the order of $\chi\varepsilon$, where

$$\chi = \frac{(pk)}{m\omega} \frac{\mathcal{E}}{\mathcal{E}_{cr}}, \quad (2)$$

with $k^\mu = (\omega/c, \mathbf{k})$ being the plane-wave's four-wave-vector and $\mathcal{E}_{cr} = m^2 c^3 / \hbar |e| \approx 1.3 \times 10^{16}$ V/cm being the so-called “critical field” of QED [4, 5]. The above estimate of the typical energy of the emitted photon is valid for $\chi \lesssim 1$. A constant and uniform electric field of the order of \mathcal{E}_{cr} provides an e^-e^+ pair with an energy comparable to its rest energy $2mc^2$ on a distance of the order of λ_C , such that the QED vacuum becomes unstable in the presence of such a strong field under e^-e^+ pair creation [7–9]. The parameter χ controls the importance of photon recoil, which becomes essential at $\chi \gtrsim 1$. The emission of a single photon in the regime $\xi, \chi \gtrsim 1$ is known as nonlinear single Compton scattering and it has been studied thoroughly in the literature [10–25].

Although initial electron wave-packets have been considered in some studies about Thomson scattering [26], and the general problem of the radiation emitted by a classical distribution of charges is a well-known problem in the Free-Electron-Laser community [27], in the study of nonlinear Compton scattering, to the knowledge of the authors, the initial state of the electron has been mostly taken as having a definite momentum. In experiments, however, an electron in a beam has some characteristic indeterminacy in the momentum and is localized to some extent; motivated by this fact, we will consider below that the electron is initially in a superposition of states of different momenta, i.e., in a wave-packet, and, among other aspects, we study whether it is possible to observe interference effects among different

components of the wave-packet. We do this in the framework of strong-field QED within the Furry picture [4–6, 28]. In [29] a scalar QED calculation with an initial particle described by a wave-packet shows how for nonlinear single Compton scattering in a monochromatic plane-wave electromagnetic field the different components of the electron wave-packet do not interfere. This result has been extended in [30] to spinor QED in pulsed fields. We will show in the following a different derivation of the same result, and in addition we will investigate in detail the effects of the initial electron’s wave-packet on the emitted radiation.

Peak laser intensities have been recently increasing dramatically due to the development of two techniques, Chirped Pulse Amplification (CPA) [31] and Optical Parametric Chirped Pulse Amplification (OPCPA) [32]. All today’s most intense lasers, like Vulcan [33], Astra-Gemini [34], HERCULES [35], Berkeley Lab Laser Accelerator (BELLA) [36], and planned ones, such as the Extreme Light Infrastructure [37], the High Power Laser Energy Research facility [38], APOLLON [39], and the Exawatt Center for Extreme Light Studies (XCELS) [40], are based on either one of these techniques. Both CPA and OPCPA generate, after the amplification of an initial pulse, an ultrashort laser pulse; it is thus likely that this kind of pulses will be adopted in experiments to probe the nonlinear QED regime. Thus, we will consider the laser field in our calculations to be an ultrashort pulse.

To the current date, the record for the highest laser intensity ever achieved is held by the HERCULES facility, that reached a peak intensity of 2×10^{22} W/cm² ($\xi \approx 70$ at $\hbar\omega = 1.55$ eV), and lasers with peak intensity $\xi \gtrsim 1$ are readily available in many facilities. It is harder, however, to reach values of the parameter χ close to unity. Starting from Eq. (2), and substituting the previously given definition of \mathcal{E}_{cr} , one can write $\chi = \xi \hbar(pk)/m^2c^2$; the factor $\hbar(pk)/m^2c^2$ makes it necessary, in order to have a χ close to unity at optical frequencies, to use ultrarelativistic electrons (even for large values of $\xi \sim 100$). Nowadays, ultrarelativistic electron beams can be conveniently produced also at laser facilities via the wakefield acceleration technique [41, 42].

Although intense pulses are usually focused almost down to diffraction limit, we will model them as plane waves. This approximation is valid if the electron collides nearly head-on with the laser field and almost at the focus of the latter, provided that the transverse excursion of the electron is much smaller than the laser waist size, which occurs if $\xi mc^2 \ll \varepsilon$ [3, 43]. Within the plane-wave approximation, the approach based on the Furry picture can be conveniently applied as the Dirac equation in a plane-wave field can be solved exactly.

Approximate solutions can be also found, however, for a field of more complex structure like a Gaussian laser beam if the conditions $\xi \gg 1$ and $\xi mc^2 \ll \varepsilon$ are fulfilled [44].

In most of the numerical work performed to obtain the results in this paper, one of the main challenges is to perform integrals of highly oscillating functions; typical quadrature schemes cannot be adopted, since they become more and more inaccurate as the frequency of the oscillations of the integrand increases. Thus, we have used Filon's method [45, 46] to deal with this kind of integrals. The basic idea behind it is to put an highly oscillating integral in the form $\int_{\mathcal{I}} dx f(x) e^{iax}$, where $f(x)$ is a smooth and sufficiently well behaved function, $a \gg 1$ is a constant, and \mathcal{I} is an interval in \mathbb{R} ; then divide \mathcal{I} in some subintervals $\{\mathcal{I}_n, n \in \mathbb{N}\}$, sufficiently small that in each of them the function $f(x)$ can be accurately approximated with a quadratic polynomial. Then, in each subinterval the starting integrals are approximated by a weighted sum of terms each having the form $\int_{\mathcal{I}_n} dx x^j e^{iax}$, where $j \in \{0, 1, 2\}$, and each of these integrals can be evaluated analytically. The advantage of this method is that the accuracy of the estimate increases with increasing a .

This paper is organized as follows. In Eq. (2), we present the general theory of the scattering of an electron in a superposition of states with different momenta and a short intense laser pulse and we show that interference effects among states with different momenta are not present. In Eq. (21), we study the particular case of an electron wave-packet colliding head-on with a laser pulse and of normally distributed longitudinal momentum, while in Fig. 5 we investigate the more general case where there is also an indeterminacy on the transverse components of the momentum. Through the rest of the article, natural units ($\hbar = c = 1$) are adopted, and the electromagnetic units used are such that the QED coupling constant is $\alpha_{QED} = e^2 (\approx 1/137)$.

II. THEORY

In the computation of nonlinear single Compton scattering rates, perturbative approaches with respect to the laser field can quickly become impractical, when a sufficiently strong incoming electromagnetic field is considered. In fact, as we mentioned in the introduction, for an incoming laser field such that $\xi \gtrsim 1$ the exchange of many photons between the laser and the electron becomes important and perturbative calculations up to a very high order would be necessary. Typically, however, such intense fields consist of an enormous

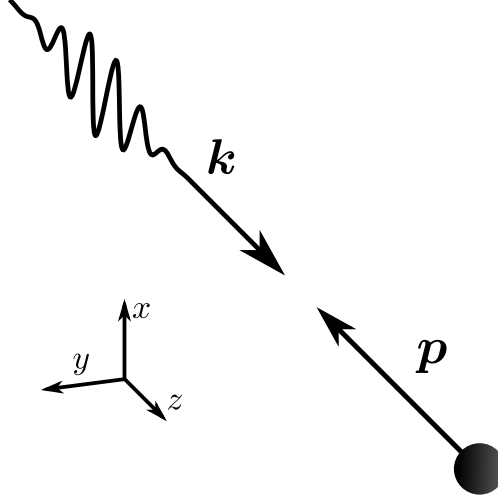


Figure 1. Representation of the choice of the employed frame of reference.

number of coherent photons; this makes it possible [3] to neglect the quantum nature of the background field and to treat it as a classical given electromagnetic field. By working within this approximation, one can split the electromagnetic field four-vector potential into two parts: a classical part, that accounts for the intense laser field, and a quantized part, that accounts for all the other excitations of the electromagnetic field, i.e., the radiation emitted by the electron. After that, the electron-positron field is quantized by taking into account exactly the background laser field. This is the so-called Furry picture of QED [3, 28], which we mentioned in the introduction, and all the following calculations are performed within this formalism.

We assume that the incoming laser field is described by the linearly-polarized plane-wave four-vector potential

$$A^\mu(\eta) = \mathcal{A}^\mu \psi(\eta). \quad (3)$$

Here, $\mathcal{A}^\mu = (0, \mathbf{\mathcal{A}})$ is a constant four-vector, where $\mathbf{\mathcal{A}}$ defines the laser polarization, with amplitude $\mathcal{A} = \mathcal{E}/\omega$ related to the peak laser's intensity I as $I = \omega^2 \mathcal{A}^2/4\pi = \mathcal{E}^2/4\pi$, and $\psi(\eta)$ is a function of the laser phase $\eta = (kx)$ describing the shape of the plane wave and such that $|\psi(\eta)| \sim |d\psi(\eta)/d\eta| \leq 1$. It is convenient to use a frame of reference in which one of the spatial axes (in our case the z axis, for the sake of definiteness) is directed along \mathbf{k} , and another one (without loss of generality, we can choose x) is directed along the same direction as $\mathbf{\mathcal{A}}$ (see Fig. 1). Thereby, we have $\eta = \omega(t - z) = \omega\varphi$, where $\varphi = t - z$. It is also useful to introduce a coordinate $T = (t + z)/2$, linearly independent of φ , x and y , and the

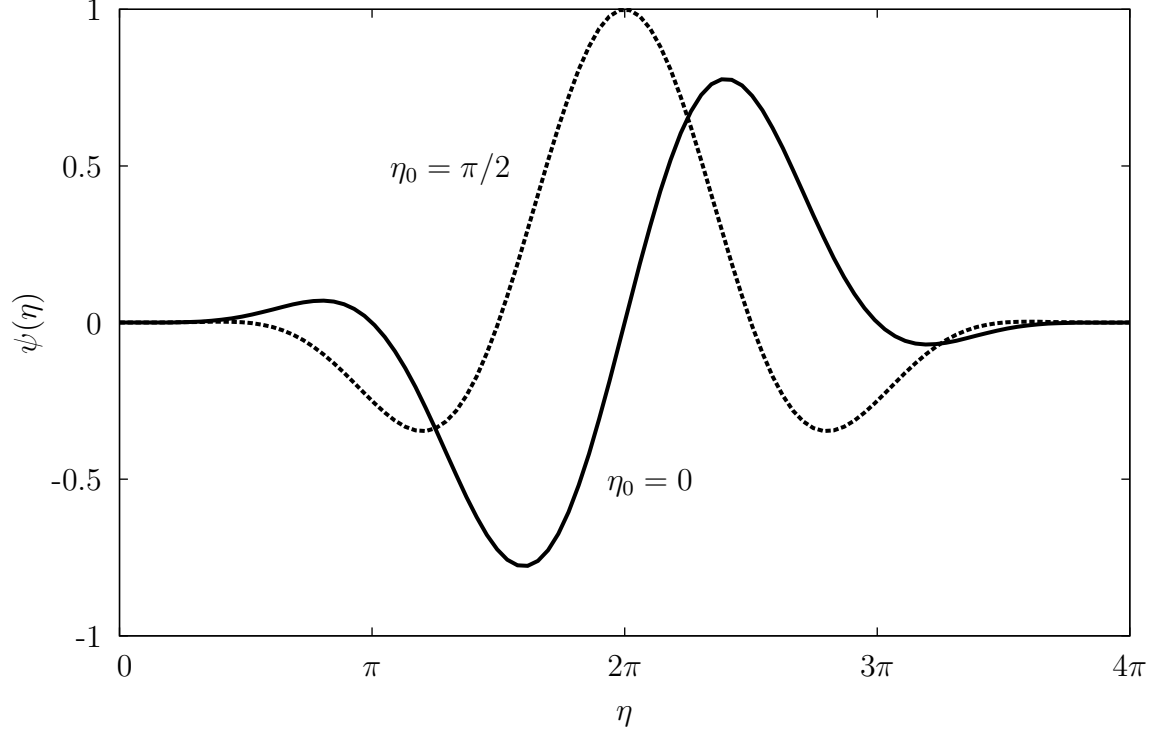


Figure 2. The function $\psi(\eta)$ for a two-cycle laser pulse ($n_C = 2$) and two choices of the carrier-envelope phase η_0 . The solid curve corresponds to $\eta_0 = 0$, while the dotted one corresponds to $\eta_0 = \pi/2$.

quantities φ , T , x and y provide the so-called light-cone coordinates of the space-time point x^μ (the factor of $1/2$ in the definition of T is arbitrary and we have chosen it in order for the Jacobian of the transformation from Cartesian coordinates to light-cone ones to be unity). In the following, we will define the $-$ (minus) contravariant component of any four-vector q^μ to be $q^- = q^0 - q^3$.

In the expression of $A^\mu(\eta)$ we have introduced the shape function $\psi(\eta)$ in order to model short laser pulses; a typically chosen [18] shape function $\psi(\eta)$ for this purpose is (see Fig. 2)

$$\psi(\eta) = \begin{cases} \sin^4\left(\frac{\eta}{2n_C}\right) \sin(\eta + \eta_0) & \text{if } \eta \in [0, 2\pi n_C], \\ 0 & \text{otherwise.} \end{cases} \quad (4)$$

In this parametrization of the laser field we have introduced the parameters n_C , the number of cycles contained in the laser pulse, and η_0 , the carrier-envelope phase (CEP) of the laser pulse. In all the numerical calculations in the following, we will chose $\eta_0 = 0$, $n_c = 2$, and $\omega = 1.55$ eV.

In the Furry picture, the states of the electron are described by the solutions of the Dirac equation in the presence of the background field; if this field is the plane wave $A^\mu(\eta)$, these solutions (known as Volkov states) are given by [3, 47]

$$\Psi_{p,\sigma}(x) = \left[1 + \frac{e}{2(kp)} \not{k} \not{A}(\eta) \right] u_{p,\sigma} e^{-ipx - i \int_{-\infty}^{\eta} \left[\frac{e}{(kp)} (pA(\eta')) - \frac{e^2}{2(kp)} A^2(\eta') \right] d\eta'}, \quad (5)$$

where the slash on a four-vectorial quantity is a shorthand notation for a contraction of that four-vector with the Dirac matrices γ^μ , that is, $\not{a} = \gamma^\mu a_\mu$ and $u_{p,\sigma}$ is a positive-energy spinor solution of the free Dirac equation $(\not{p} - m) u_{p,\sigma} = 0$, with $\bar{u}_{p,\sigma} u_{p,\sigma} = 2m$ ($\bar{u}_{p,\sigma} = u_{p,\sigma}^\dagger \gamma^0$). The Volkov state $\Psi_{p,\sigma}(x)$ is characterized by the four-momentum $p^\mu = (\varepsilon, \mathbf{p})$ ($\varepsilon = \sqrt{m^2 + |\mathbf{p}|^2}$) and by the spin quantum number σ at $t \rightarrow -\infty$ (these are the so-called Volkov in-states, although Volkov out-state only differ from the in-ones by a phase independent of the coordinates). The Volkov states in Eq. (5) are normalized as

$$\int d^3x \Psi_{p',\sigma'}^\dagger(x) \Psi_{p,\sigma}(x) = (2\pi)^3 (2\varepsilon) \delta(\mathbf{p} - \mathbf{p}') \delta_{\sigma,\sigma'}. \quad (6)$$

As we have mentioned in the introduction, we consider an electron state which is a wave-packet made of a superposition of Volkov states with different momenta and a given spin number σ :

$$\Phi_\sigma(x) = \int \frac{d^3p}{(2\pi)^3(2\varepsilon)} \rho(\mathbf{p}) \Psi_{p,\sigma}(x). \quad (7)$$

Here, $\rho(\mathbf{p})$ is a complex-valued, scalar weighting function; in order for the state $\Phi_\sigma(x)$ to be normalized to unity, $\rho(\mathbf{p})$ needs to be normalized in a covariant way as

$$\int \frac{d^3p}{(2\pi)^3(2\varepsilon)} |\rho(\mathbf{p})|^2 = 1. \quad (8)$$

The leading order S -matrix element relative to the process of the emission of a photon, with wave four-vector $k'^\mu = (\omega', \mathbf{k}')$ and polarization four-vector $\epsilon_l'^\mu$, by an electron in the initial state $\Phi_\sigma(x)$ is

$$S_{fi} = -ie\sqrt{4\pi} \int d^4x \frac{d^3p}{(2\pi)^3(2\varepsilon)} \rho(\mathbf{p}) \bar{\Psi}_{p',\sigma'}(x) \not{\epsilon}_l'^* e^{ik'x} \Psi_{p,\sigma}(x). \quad (9)$$

We notice that among the space-time coordinates the integrand in Eq. (9) depends non-trivially only on φ , while on the other three space-time coordinates we have integrals that evaluate to three delta functions. It is thus possible [18] to write S_{fi} in the form

$$S_{fi} = -ie\sqrt{4\pi} (2\pi)^3 \int \frac{d^3p}{(2\pi)^3(2\varepsilon)} \rho(\mathbf{p}) (\bar{u}_{p',\sigma'} M_{fi} u_{p,\sigma}) \delta^{(-,x,y)}(p - k' - p'); \quad (10)$$

here, $\delta^{(-,x,y)}(p - k' - p')$ is a three dimensional Dirac delta that ensures the conservation of the three contravariant components $-$, x and y of the total four-momentum and

$$M_{fi} = \epsilon_l'^* f_0 + e \left(\frac{\mathcal{A} k \epsilon_l'^*}{2(kp')} + \frac{\epsilon_l'^* k \mathcal{A}}{2(kp)} \right) f_1 - \frac{e^2 \mathcal{A}^2 (k \epsilon_l'^*) k}{2(kp)(kp')} f_2, \quad (11)$$

$$f_j = \int_{-\infty}^{+\infty} d\eta \psi^j(\eta) e^{i \int_{-\infty}^{\eta} d\eta' [\alpha \psi(\eta') + \beta \psi^2(\eta') + \gamma]}. \quad (12)$$

In Eq. (12) we have introduced the three parameters [48]

$$\alpha = e \left[\frac{(p' \mathcal{A})}{(kp')} - \frac{(p \mathcal{A})}{(kp)} \right], \quad (13)$$

$$\beta = -\frac{e^2 \mathcal{A}^2}{2} \frac{(k' k)}{(kp)(kp')}, \quad (14)$$

$$\gamma = \frac{(pk')}{(p'k)}. \quad (15)$$

In order to compute emission rates, it is necessary to calculate the square modulus of S_{fi} :

$$|S_{fi}|^2 = 4\pi e^2 \int \frac{d^3 p}{(2\varepsilon)} \frac{d^3 \tilde{p}}{(2\tilde{\varepsilon})} \rho^*(\tilde{\mathbf{p}}) \rho(\mathbf{p}) (\bar{u}_{p',\sigma'} M_{fi} u_{\tilde{p},\sigma})^* (\bar{u}_{p',\sigma'} M_{fi} u_{p,\sigma}) \times \delta^{(-,x,y)}(p - k' - p') \delta^{(-,x,y)}(\tilde{p} - k' - p'). \quad (16)$$

The integrations in Eq. (16) are along the components of \mathbf{p} and $\tilde{\mathbf{p}}$ in Cartesian coordinates, while one of the delta functions in Eq. (16) is expressed in terms of light-cone coordinates. An easy way to perform these integrations is to change the measure for each momentum integration from $dp_x dp_y dp_z = d^2 p_\perp dp_z$ to $d^2 p_\perp dp^-$; the Jacobian one has to insert for this transformation is ε/p^- . Thus one can start from Eq. (16), change the integration measure to $d^2 p_\perp dp^- d^2 \tilde{p}_\perp d\tilde{p}^-$, perform the integrations in \tilde{p} (that are just integrations of delta functions), and change back the measure to $d^3 p$; this gives

$$|S_{fi}|^2 = 4\pi e^2 \int \frac{d^3 p}{(2\varepsilon)(2p^-)} |\rho(\mathbf{p})|^2 |\bar{u}_{p',\sigma'} M_{fi} u_{p,\sigma}|^2 \delta^{(-,x,y)}(p - k' - p'). \quad (17)$$

The unpolarized emission rate is obtained by integrating $|S_{fi}|^2$ over the electron's final momentum and on the wave-vector of the emitted photon, and by summing over the final electron spin and photon polarization, and averaging on the initial electron spin [2, 3]:

$$dW = \frac{d^3 k}{(2\pi)^3 (2\omega')} \int \frac{d^3 p'}{(2\pi)^3 (2\varepsilon')} \frac{d^3 p}{(2\varepsilon)(2p^-)} 4\pi e^2 |\rho(\mathbf{p})|^2 \delta^{(-,x,y)}(p - k' - p') \frac{1}{2} \sum_{\sigma, \sigma', l} |\bar{u}_{p',\sigma'} M_{fi} u_{p,\sigma}|^2. \quad (18)$$

The integral on d^3p' can be readily evaluated with the same change of integration measure previously mentioned. By writing $d^3k' = \omega'^2 d\omega' d\Omega'$ and remembering that the emission rate and the energy emission rate are related by $dE = \omega' dW$, it is possible to write the angular differential emission rate as

$$\frac{dE}{d\omega' d\Omega'} = \int \frac{d^3p}{(2\pi)^3 (2\varepsilon)} |\rho(\mathbf{p})|^2 \frac{e^2 \omega'^2}{2(4\pi)^2 p^- q^-} \sum_{\sigma, \sigma', l} |\bar{u}_{q, \sigma'} M_{fi} u_{p, \sigma}|^2, \quad (19)$$

where q^μ is a four vector such that $q^- = p^- - k'^-$, $q_{x,y} = p_{x,y} - k'_{x,y}$ and $q^+ = (q^0 + q^3)/2 = (m^2 + q_x^2 + q_y^2)/2q^-$ ($q^2 = m^2$). Equation (19) can be easily identified as the incoherent average over the modulus squared of $\rho(\mathbf{p})$ of the well-known expression of the differential angular energy emission rate for a nonlinear single Compton scattering event of an electron with definite initial four-momentum p^μ and final four-momentum q^μ [14, 18, 48]

$$\frac{dE_p}{d\omega' d\Omega'} = \frac{e^2 \omega'^2}{2(4\pi)^2 p^- q^-} \sum_{\sigma, \sigma', l} |\bar{u}_{q, \sigma'} M_{fi} u_{p, \sigma}|^2. \quad (20)$$

Thus, there are no quantum interference effects between initial states of the electron having different values of the momentum. The physical reason behind the absence of interference is that, in principle, by measuring the final state of the electron and of the emitted photon one can retrieve the initial momentum of the electron, and so the initial state of the electron amongst the ones contained in the initial superposition.

The results we presented so far allow us to state that, as far as one is interested in nonlinear single Compton scattering rates, the state of the initial electron can be described equivalently either with a superposition of states like the one in Eq. (7) or as a statistical mixture

$$\hat{\rho}_\sigma = \int \frac{d^3p}{(2\pi)^3 (2\varepsilon)} |\rho(\mathbf{p})|^2 |\Psi_{p, \sigma}\rangle \langle \Psi_{p, \sigma}| \quad (21)$$

where the weighting function $\rho(\mathbf{p})$ is the same of Eq. (7) and $\Psi_{p, \sigma}(x) = \langle x | \Psi_{p, \sigma} \rangle$.

III. ELECTRON WAVE-PACKETS WITH NORMALLY DISTRIBUTED LONGITUDINAL MOMENTUM

After describing the theory for arbitrary superpositions of Volkov states (for a given spin quantum number), in this section and in the next one we will make an explicit choice of $\rho(\mathbf{p})$. Let the initial state of the electron be a superposition of states with momenta always

directed almost in the opposite direction of the laser wave-vector \mathbf{k} (for the choice of the frame of reference we adopted in Eq. (2), i.e., the momenta \mathbf{p} are all directed almost along the negative z direction). In particular, we assume that the distribution of the momenta is a triple Gaussian distribution, with average momentum $\bar{\mathbf{p}} = (0, 0, \bar{p}_z)$, with $\bar{p}_z < 0$, and with variance $\sigma_{p_T}^2$ along the x and y direction and $\sigma_{p_z}^2$ along the z -direction; thus the initial wave-packet is given by

$$\Phi_\sigma(x) = \int \frac{d^3p}{(2\pi)^3 (2\varepsilon)} \frac{1}{\sigma_{p_T} \sqrt[4]{\sigma_{p_z}^2} (2\pi)^3} e^{-\frac{(p_z - \bar{p}_z)^2}{4\sigma_{p_z}^2}} e^{-\frac{p_x^2 + p_y^2}{4\sigma_{p_T}^2}} \Psi_{p,\sigma}(x). \quad (22)$$

In the present section the transverse variance $\sigma_{p_T}^2$ is assumed to be sufficiently small, so that all transverse momenta (p_x, p_y) in Eq. (19) can be set equal to zero (except than in the exponential in Eq. (22)). Thus, the electron effectively collides head-on with the laser beam.

In order to understand the modifications brought about by the electron being described by the wave-packet in Eq. (22), we plot in Fig. 3 the emission spectrum in the forward (negative z) direction for an incoming electron with definite momentum with components $p_x = p_y = 0$, and $p_z = -4.2$ GeV ($\varepsilon \approx 4.2$ GeV) [42] interacting with a laser of intensity $I \approx 4.3 \times 10^{20}$ W/cm². The above parameters correspond to $\xi = 10$ and $\chi \approx 0.50$. The spectra in the regime of $|p_z| \gg m$ and $\xi \gg 1$ exhibit a large number of narrow peaks. The position of the peaks depends on the momentum of the electron; in particular, from Fig. 4 one can deduce that, as the electron's initial momentum increases in modulus, these peaks will be shifted towards higher frequencies. These shifts depend on the position of the peaks itself, i.e., different peaks are shifted by a different amount, when changing p_z . More specifically, by changing p_z of the same amount, the higher peak frequencies will be shifted more than the lower ones. The above results can be easily explained as a result of the Doppler effect. For the sake of simplicity we consider here the idealized case of a monochromatic laser field (with laser photon energy ω). In this case, in fact, the frequency of the n^{th} harmonic emission along the negative z direction is given by [4]

$$\omega'_n = \frac{n(pk)}{(pn') + \left(n + \frac{m^2 \xi^2}{4(pk)}\right) (kn')} = \frac{n\omega (\varepsilon - p_z)^2}{m^2 \left(1 + \frac{\xi^2}{2}\right) + 2n\omega(\varepsilon - p_z)} = \frac{\zeta_n}{1 + 2\zeta_n}(\varepsilon - p_z), \quad (23)$$

where $n'^\mu = (1, \mathbf{k}'/\omega') = (1, 0, 0, -1)$ and where we have introduced the dimensionless pa-

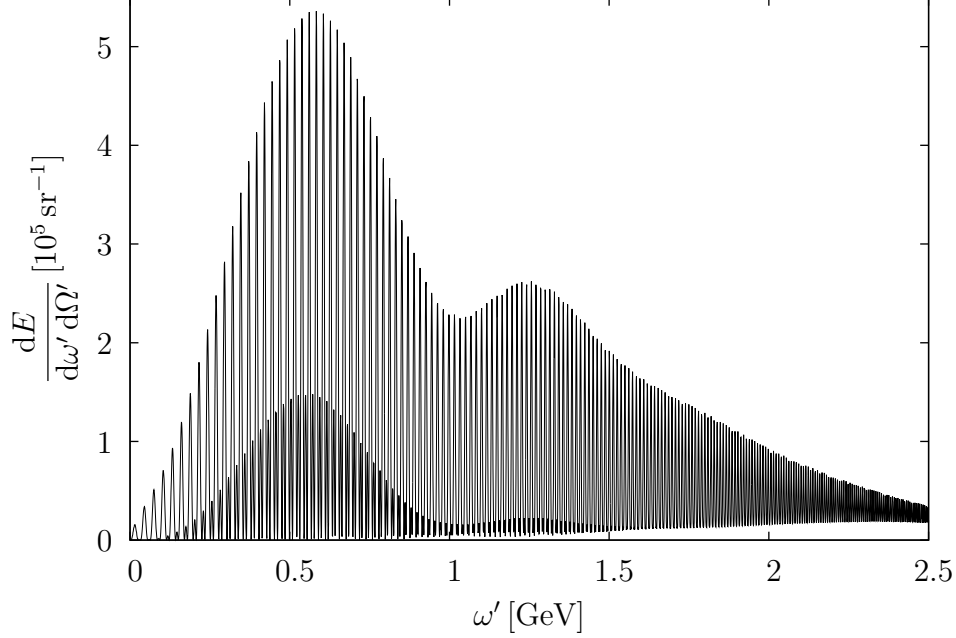


Figure 3. Energy emission spectrum along the negative z -direction for an incoming electron with definite initial momentum $\mathbf{p} = (0, 0, -4.2 \text{ GeV})$ interacting with a laser of intensity $I \approx 4.3 \times 10^{20} \text{ W/cm}^2$.

parameter

$$\zeta_n = \frac{n\omega(\varepsilon - p_z)}{m^2 \left(1 + \frac{\xi^2}{2}\right)}. \quad (24)$$

By means of a first-order expansion with respect to the shift Δp_z , we can estimate the relative shift of these frequencies when slightly changing the value of p_z :

$$\frac{\Delta\omega'_n}{\omega'_n} = \frac{1}{\omega'_n} \frac{\partial\omega'_n}{\partial p_z} \Delta p_z = -2 \frac{1 + \zeta_n}{1 + 2\zeta_n} \frac{\Delta p_z}{\varepsilon}. \quad (25)$$

In the case of an ultrarelativistic electron and in the relevant regime $\xi \gg 1$, it is $\varepsilon \approx |p_z|$ and $\zeta_n \approx 2n\chi/\xi^3$, such that we obtain

$$\frac{\Delta\omega'_n}{\Delta|p_z|} \approx 4 \frac{\zeta_n(1 + \zeta_n)}{(1 + 2\zeta_n)^2}. \quad (26)$$

As it can be easily shown, the quantity $\Delta\omega'_n/\Delta|p_z|$ increases monotonically with the harmonic number, in agreement with the findings in Fig. 4.

Notice that Eq. (26) is valid only for a monochromatic laser field, whereas we are interested here in the case of short pulses, i.e., pulses also characterized by a certain spread $\Delta\omega$ around a central angular frequency ω . It is thus interesting to compare the relative shift due

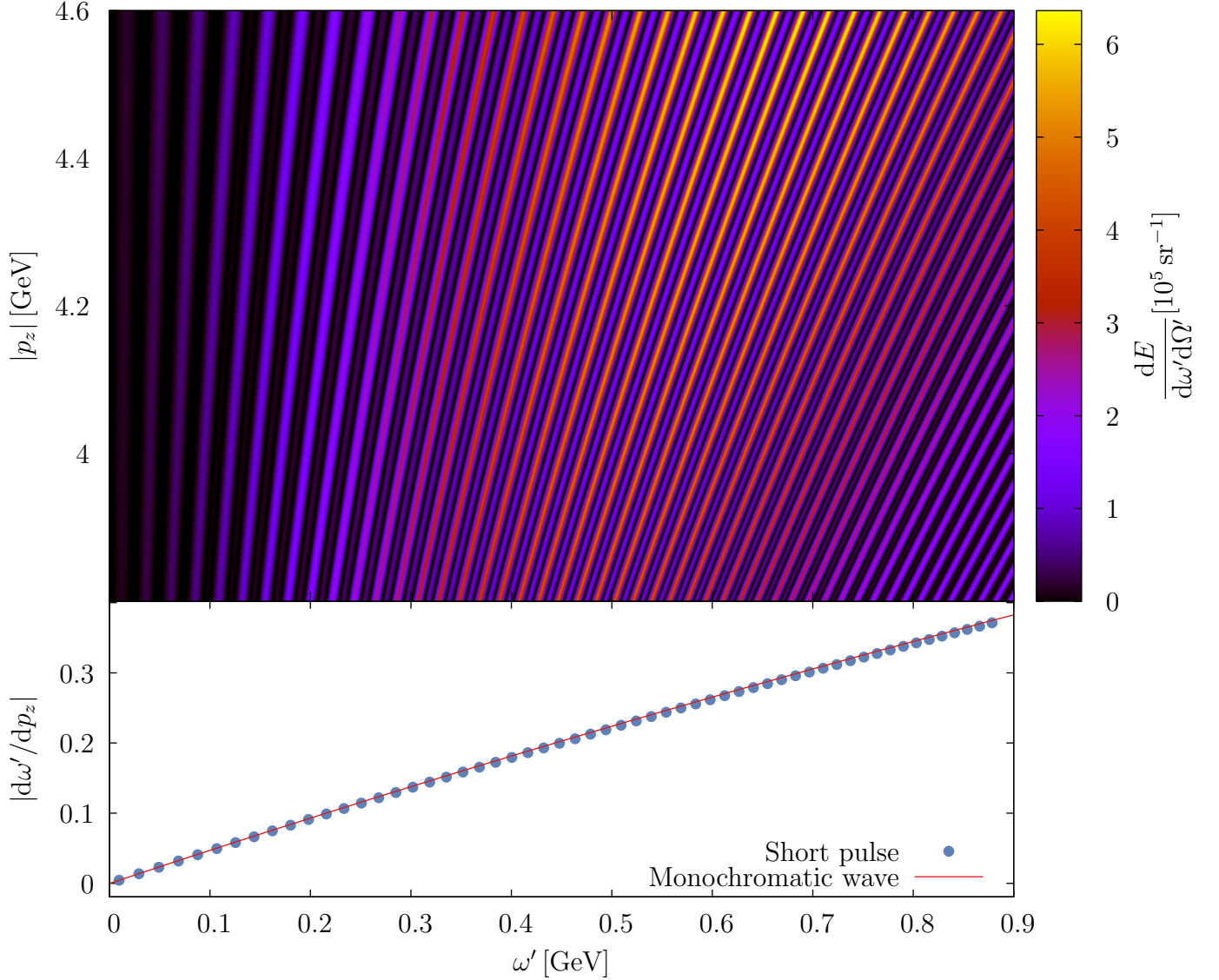


Figure 4. (color online) Change of the emission spectrum for an electron with definite initial momentum $(0, 0, p_z)$ as a function of $|p_z|$ (Fig. 3 corresponds to a section of the upper part of this figure for $p_z = -4.2$ GeV). In the range considered, the position of the peaks increases linearly with p_z , albeit with different slopes depending on the position of the peak. Some of these slopes were computed numerically and are shown in the bottom part of the plot (blue dots), together with the same quantity computed analytically for a monochromatic pulse (red continuous line).

to an uncertainty of p_z to the one due to an indeterminacy on the value of ω . In analogy to what we have discussed for Eq. (25), one can derive a similar relation, for a variation $\Delta\omega$ of the laser angular frequency. By adding the resulting expression to Eq. (25) and by assuming again that $|\bar{p}_z| \gg m$ and $\xi \gg 1$, it is possible to obtain the first-order relative variation of

ω'_n with respect to the relative variations of ω and p_z as:

$$\frac{\Delta\omega'_n}{\omega'_n} \approx \frac{1}{1+2\zeta_n} \frac{\Delta\omega}{\omega} + 2 \frac{1+\zeta_n}{1+2\zeta_n} \frac{\Delta|p_z|}{|p_z|}. \quad (27)$$

Since $\zeta_n > 0$ it is clear that for comparable relative variations in ω and p_z , the induced shift due to the spread in the incoming electron momentum is larger. From the aforementioned properties of the emitted photon's spectrum of a monochromatic initial electron we can infer the final spectrum when the state $\Phi_\sigma(x)$ of Eq. (7) is considered, since the emission spectrum resulting from that state, as it was shown above, is a weighted average of monochromatic emission spectra with different p_z . The sharp peaks present in the spectrum for a fixed value of p_z will be differently shifted and will tend to fill the valleys present in the spectrum relative to another value of p_z ; when averaging many of these spectra, the net effect is a smoothing of the final spectra and a decrease of the yield as compared to the latter obtained at the peaks in the monochromatic case.

Moreover, we have already mentioned the fact that the shift induced by the spread in the electron momentum is larger for higher emission frequencies. Thus, the portion of the spectrum that will be smoothed earlier, i.e., even for relatively small values of σ_{p_z} , is that at high frequencies of the emitted photon. Indeed, this is the result we obtain in Fig. 5, where the final photon energy spectrum for different values of σ_{p_z} is plotted (the numerical parameters are the same as in Fig. 3 and the average value of the initial momentum of the electron is $\bar{\mathbf{p}} = (0, 0, -4.2 \text{ GeV})$). We have chosen values of the standard deviation σ_{p_z} equal to 0.5%, 1% or 5% of the incoming momentum, corresponding to 21 MeV, 42 MeV or 210 MeV, respectively. Even when the relative indeterminacy on the momentum is only 0.5%, we can see that the height of the highest peaks is reduced by a factor of about two, and all the oscillatory features at $\omega' \gtrsim 1 \text{ GeV}$ are completely washed out (see Fig. 3 and Fig. 5). For larger values of σ_{p_z} , these effects are even more evident also for the lowest part of the spectrum. Concerning the choice of σ_{p_z} and in general of the properties of the wave-packet $\Phi_\sigma(x)$ a comment is in order. In fact, in general, the state $\Phi_\sigma(x)$ describes a single electron. The properties of the corresponding wave-packet depend on how the electron is produced and accelerated [49], and are in principle different from, for example, the corresponding properties of an electron bunch. However, in our case, as we have seen, the spectra for the state $\Phi_\sigma(x)$ coincide with those obtained by considering a corresponding electron bunch with an average electron number equal to unity. In this respect, the values

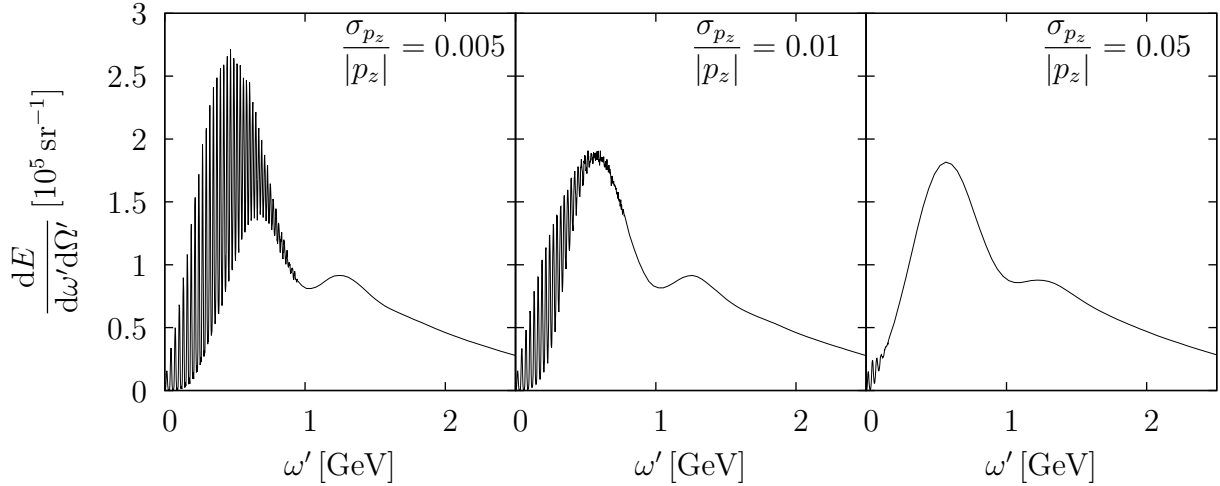


Figure 5. Emission spectra along the negative z -direction for an electron wave-packet with $\bar{\mathbf{p}} = (0, 0, -4.2 \text{ GeV})$ interacting with a laser pulse of peak intensity $I \approx 4.3 \times 10^{20} \text{ W/cm}^2$ for different values of the spread of the longitudinal momentum.

of the momenta spreads are chosen according to the features of electron beams, which can be obtained presently experimentally [42].

IV. MULTIVARIATE GAUSSIAN WAVE-PACKETS

We now turn our attention to the experimentally more realistic situation of an electron wave-packet that can have also non-zero components of the transverse momentum. Our choice for the initial state is as in Eq. (22) but this time the variance $\sigma_{p_T}^2$ is assumed not to be small. Also in this case, as we did in the previous section, we will first consider how the spectrum of electrons initially in a Volkov state in a monochromatic field is modified as a function of the components of the initial momentum. Then, starting from those considerations, we will focus onto the case of an electron wave-packet in a short laser pulse.

In order to understand how the emission spectrum is altered by the possibly non-zero value of the transverse components of the initial momentum, we show how the harmonic frequencies along the negative z -direction are shifted as the transverse momentum $p_T = \sqrt{p_x^2 + p_y^2}$ varies. We can thus proceed in analogy to the derivation of Eq. (26). The starting point is the initial form of ω'_n in Eq. (23), which can be rewritten in the more convenient

form

$$\omega'_n = \frac{n\omega(\varepsilon - p_z)^2}{m^2 \left(1 + \frac{\xi^2}{2}\right) + p_T^2 + 2n\omega(\varepsilon - p_z)}, \quad (28)$$

showing the explicit dependence also on p_T^2 (remember that now also the energy ε depends on p_T^2). By expanding ω'_n around $p_T = 0$ we obtain

$$\frac{\Delta\omega'_n}{\omega'_n} = \frac{1 - (\varepsilon/n\omega - 1)\zeta_n}{1 + 2\zeta_n} \frac{\Delta p_T^2}{\varepsilon(\varepsilon - p_z)}, \quad (29)$$

where all the energies are calculated at $p_T = 0$. This equation shows that again the relative shift depends on the harmonic number n . In a typical scenario where $\varepsilon \approx |p_z|$ and $\xi \gg 1$, the same approximations as in the previous section can be applied. The result for $\Delta\omega'_n$ reads

$$\Delta\omega'_n = \zeta_n \frac{1 + \zeta_n - \varepsilon\chi/\xi^3\omega}{(1 + 2\zeta_n)^2} \frac{\Delta p_T^2}{\varepsilon}, \quad (30)$$

with ζ_n given in Eq. (24), which in the current approximations ($\varepsilon \approx |p_z|$, $\xi \gg 1$) is approximately equal to $n\chi/\xi^3$. Equation (30) shows that an important role is played by the parameter $\mu = \varepsilon\chi/\xi^3\omega$. If we work in the quantum regime where $\chi \sim 1$, since at $\xi \sim 10^2$ electron energies in the GeV-range are required, we can safely assume that $\mu \gg 1$. Moreover, at $\zeta_n \gg 1$ the emission spectrum is suppressed [4] such that we can conveniently further approximate the expression for $\Delta\omega'_n$ as

$$\Delta\omega'_n = -\frac{\varepsilon\chi}{\xi^3\omega} \frac{\zeta_n}{(1 + 2\zeta_n)^2} \frac{\Delta p_T^2}{\varepsilon}. \quad (31)$$

This expression indicates that we would expect a negative shift of the harmonics, which becomes less pronounced at $\zeta_n \ll 1$ (low harmonics) and at $\zeta_n \gg 1$ (high harmonics). This is exactly what we observe in Fig. 6, where different curves $\omega'_n = \omega'_n(p_T)$ for different values of n are plotted, with the numerical parameters: $p_z = -4.2$ GeV and $I \approx 1.1 \times 10^{20}$ W/cm² ($\xi = 5$, $\chi \approx 0.25$, and $\mu \approx 5.4 \times 10^6$).

A typical collection of monochromatic electron spectra along the forward direction is shown in Fig. 7 by electrons having initially $p_z = -4.2$ GeV and either $p_y = 0$ or $p_x = 0$ (we recall that p_x (p_y) is the component of the momentum along the direction of the electric (magnetic) field of the laser), interacting with a short laser pulse with $I \approx 1.1 \times 10^{20}$ W/cm² ($\xi = 5$, $\chi \approx 0.25$). Apart from exhibiting the already mentioned shift of the peak frequencies as one of the transverse components varies, we also observe that by varying p_y by about 1-2 electron masses the spectrum is significantly suppressed. The reason is that the observation

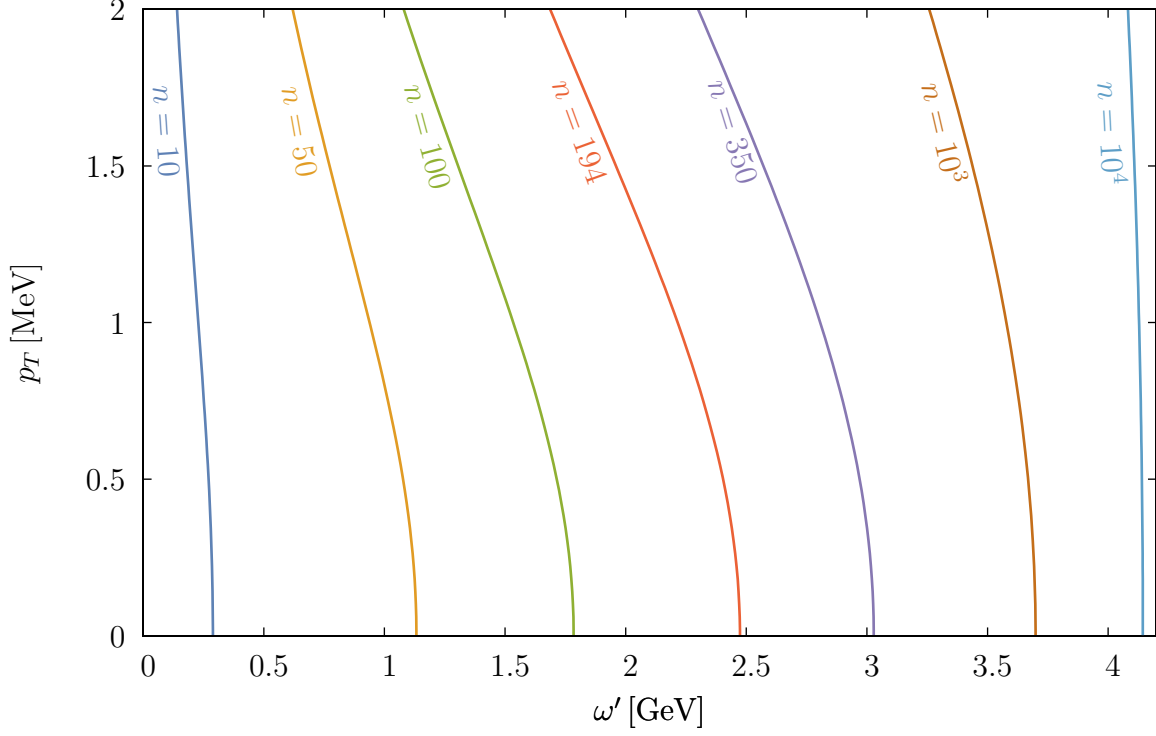


Figure 6. (color online) Shift of the emission frequencies ω'_n along the negative z -direction for different values of n as a function of p_T (vertical axis). The numerical parameters are $p_z = -4.2$ GeV and $I \approx 1.1 \times 10^{20}$ W/cm².

direction is the forward direction and that the angular emission range of the electron along the magnetic field of the laser is of about m/ε , whereas along the electric field of the laser, the electron emits up to angles of the order of $m\xi/\varepsilon$ [48]. It is also worth observing the large oscillations in the emitted intensity between successive peaks when varying p_x (top part of Fig. 7). These oscillations are expected to have an important effect, when averaging many spectra, even for $|p_x| \ll m\xi$.

The above observations are confirmed by numerical calculations. In Fig. 8 (Fig. 9), we show the effects on the spectrum of the emitted photon along the negative z direction (in a direction that lies on the xz -plane, the laser polarization-propagation plane, and forms an angle $\theta = m\xi/2\bar{\varepsilon}$ with the negative z -axis, where $\bar{\varepsilon}$ is the average initial electron energy) of having either $\sigma_{p_T} \neq 0$ or $\sigma_{p_z} \neq 0$, or $\sigma_{p_T}, \sigma_{p_z} \neq 0$ (in the first two cases σ_{p_z} and σ_{p_T} , respectively, are considered to be sufficiently small that their effects can be neglected as explained below Eq. (22)).

In the numerical spectra in Fig. 8 and Fig. 9, the average initial momentum of the

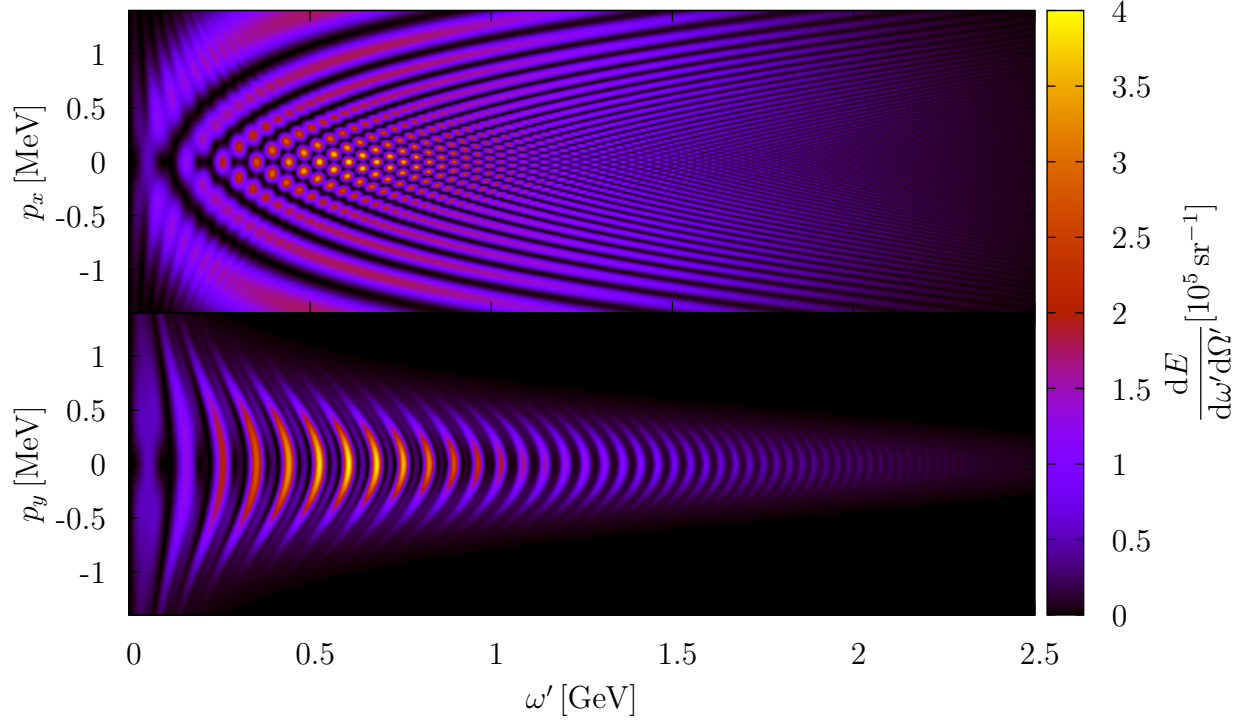


Figure 7. (color online) Emission spectra in the negative z -direction for electrons having initially $p_z = -4.2$ GeV and either $p_y = 0$ or $p_x = 0$, after the interaction with a short laser pulse with $I \approx 1.1 \times 10^{20}$ W/cm².

electron is $\bar{\mathbf{p}} = (0, 0, -4.2 \text{ GeV})$, and the indeterminacy on the transverse components is $\sigma_{p_T} = 3 \times 10^{-4} |\bar{\mathbf{p}}|$, while the one on the z -component is $\sigma_{p_z} = 6 \times 10^{-2} |\bar{\mathbf{p}}|$ (these parameters for the electron beam are compatible with those in [42]). The intensity of the laser field is $I \approx 1.1 \times 10^{20}$ W/cm² ($\xi = 5$, $\chi = \bar{\chi} \approx 0.25$ as calculated from the average electron momentum).

In Fig. 8 and Fig. 9 one can see that for the chosen values of the parameters σ_{p_T} and σ_{p_z} , the most dramatic alteration of the spectrum is due to the transverse momentum spread of the electron beam, even though its value is orders of magnitude smaller than the spread on p_z . In fact, the effect due to $\sigma_{p_T} \neq 0$ is so dominant that switching on also the longitudinal spread σ_{p_z} has no observable effect on the emitted spectrum (the dotted red curve is on top of the short-dashed orange one in both Fig. 8 and Fig. 9). As a result, the finer structures in the spectra are washed out and, in this respect, in order to at least partially observe them one should experimentally render the incoming electron beam as collimated as possible.

We also show in Fig. 10 the energy emission along a direction that lies on the laser po-

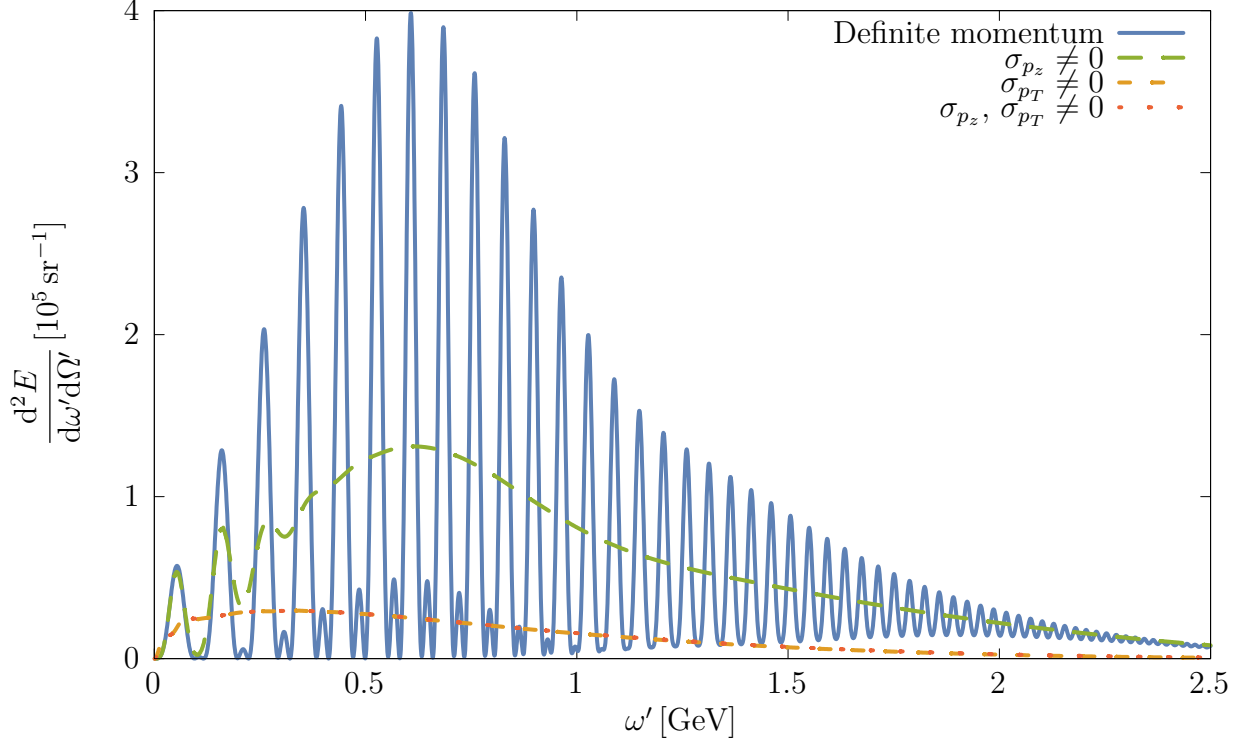


Figure 8. (color online) Energy emission spectrum in the negative z -direction, for some different initial electron states. Here, $\bar{\mathbf{p}} = (0, 0, -4.2 \text{ GeV})$, $\sigma_{p_T} = 3 \times 10^{-4} |\bar{\mathbf{p}}|$, and $\sigma_{p_z} = 6 \times 10^{-2} |\bar{\mathbf{p}}|$. The intensity of the laser field is $I \approx 1.1 \times 10^{20} \text{ W/cm}^2$.

larization plane and forms an angle $m\xi/2\bar{\varepsilon}$ with the negative z -axis for $\chi = \bar{\chi} \approx 0.85$ (the parameters used for Fig. 10 are the same of Fig. 9, except that $I \approx 1.2 \times 10^{21} \text{ W/cm}^2$ corresponding to $\xi = 17$); the qualitative behavior for nonzero values of σ_{p_z} and σ_{p_T} is the same as the one previously discussed. We should emphasize that, as we have already mentioned in the discussion below Eq. (31), the larger effect due to the transverse momentum uncertainty is also related to the fact that the considered spectra refer to some specific observation directions. In fact, if we integrate with respect to the emission angles the spectrum corresponding to the numerical parameters in Fig. 10, we obtain the results in Fig. 11; they show that the total emitted energy as a function of ω' changes only at frequencies $\omega' \approx \bar{\varepsilon} = 4.2 \text{ GeV}$ and that it is almost not affected by the momentum spreading of the incoming wave-packet. The higher rates observed at these frequencies in the case of a wave-packet with $\sigma_{p_z} \neq 0$ (see inset of Fig. 11) can be explained as some components of the wave-packet have energies larger than $\bar{\varepsilon}$.

In order to analyze the properties of the emitted radiation in the spatial domain, one

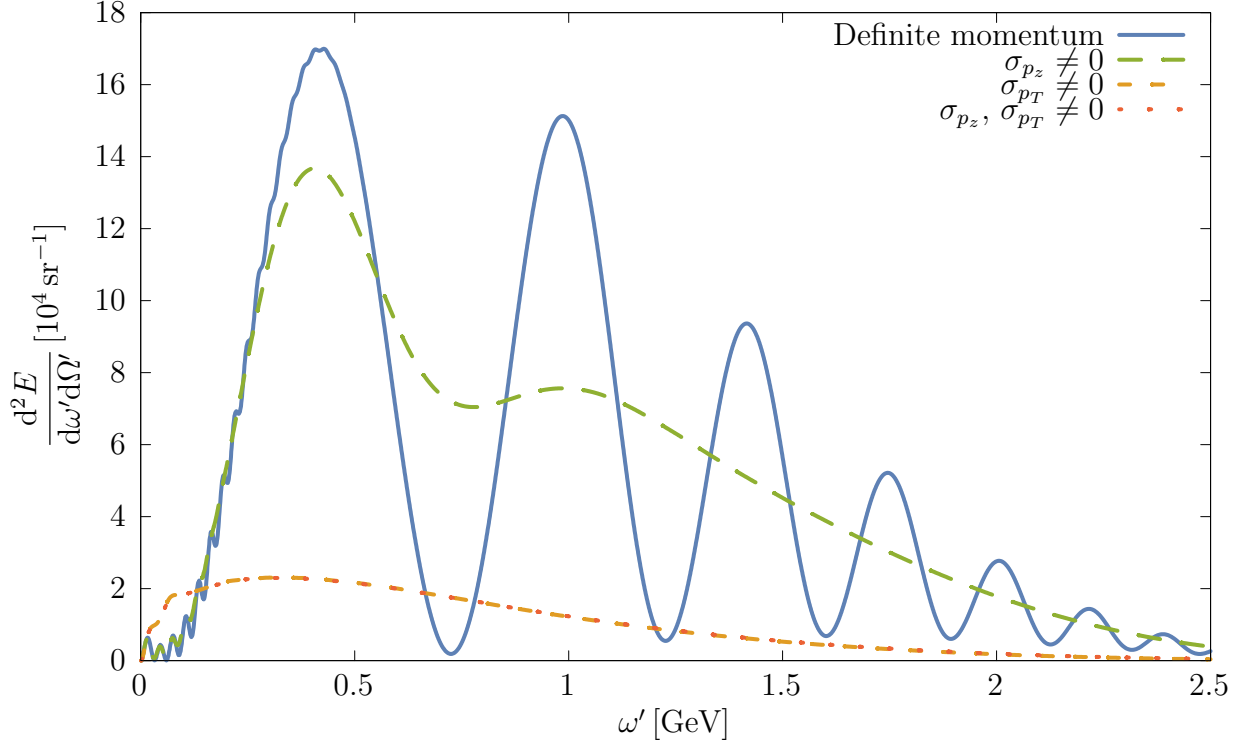


Figure 9. (color online) Energy emission spectrum on a direction in the xz -plane forming an angle $\theta = m\xi/2\varepsilon$ with the negative z -axis, for some different initial electron states. The numerical parameters are the same as in Fig. 8.

can integrate $dE/d\omega' d\Omega'$ with respect to ω' and obtain the total energy emitted along each direction. A typical result of this procedure is shown in Fig. 12. On the right panel the energy emitted per steradian by an electron in a Gaussian wave-packet is plotted (the numerical parameters are the same as in Fig. 10). The left panel shows the same quantity but emitted by an electron in a Volkov state with a definite momentum given by the $\bar{\mathbf{p}}$ of the mentioned Gaussian wave-packet. In Fig. 12 the polar angle θ and the azimuthal angle ϕ are indicated assuming the negative z -axis as polar axis. As mentioned above, when the electron is initially in a pure Volkov state, and the laser is linearly polarized, the angular aperture of the emitted radiation is $m\xi/\varepsilon$ (m/ε) along the polarization (magnetic-field) direction, which is confirmed by the the left panel in Fig. 12. The emission in the case of a multivariate Gaussian wave-packet, in the right panel of Fig. 12, extends over a broader region and is thus less intense, in the regime where σ_{p_T} and σ_{p_z} are much smaller than $|\bar{p}_z| \gg m$. In fact, at $\xi \gg 1$, if $\sigma_{p_T} \ll |\bar{p}_z|$ and $\sigma_{p_z} \ll |\bar{p}_z|$, the total energy emitted when the electron is either in a Volkov state or in a Gaussian wave-packet is almost the same (see Fig. 11). Then, as

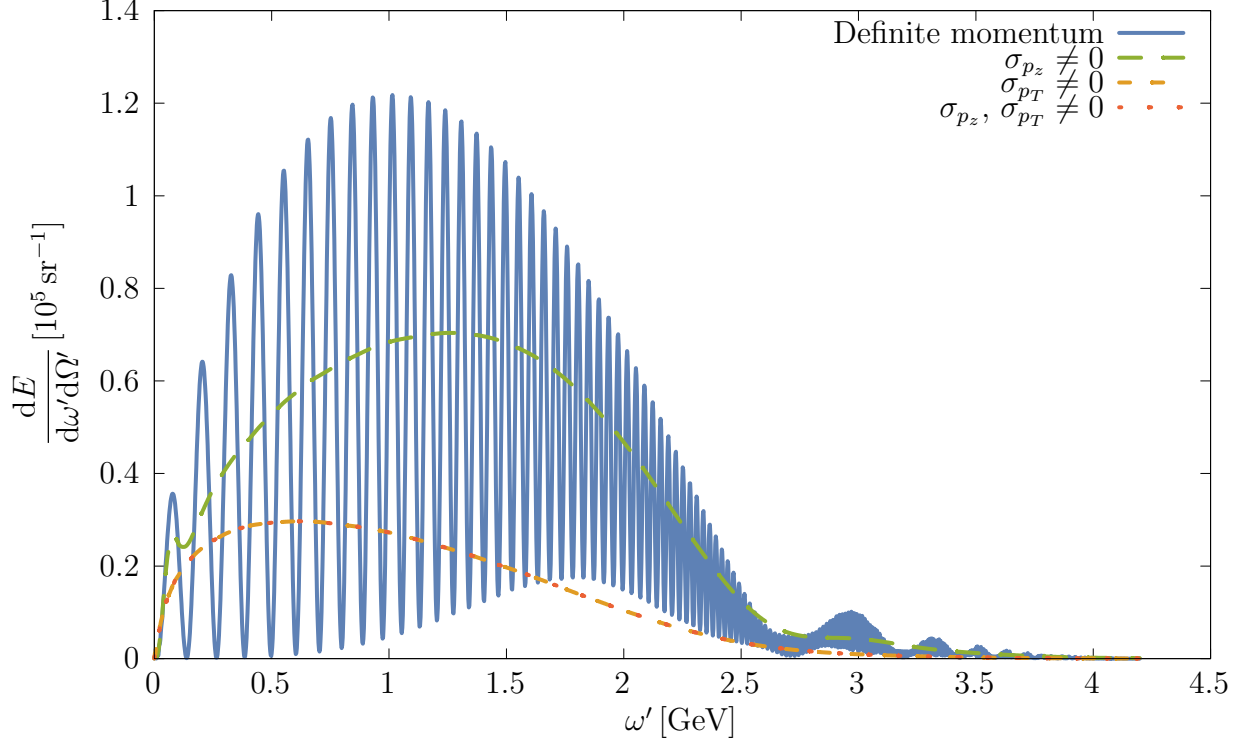


Figure 10. (color online) Energy emission spectrum for an electron wave-packet in the quantum regime ($\chi \approx 0.85$), in the direction that lies on the laser polarization plane and forms an angle $m\xi/2\bar{\varepsilon}$ with the negative z-axis. The numerical parameters are the same as in Fig. 8, except that $I \approx 1.2 \times 10^{21}$ W/cm².

the region of emission becomes broader, the radiation intensity in the Gaussian wave-packet case decreases. We briefly notice here that this effect might be also exploited in principle as a diagnostic tool of the momentum spreading of the electron beam, provided that the laser parameters like its intensity are known with sufficiently high accuracy.

V. CONCLUSIONS

In the present article we have studied nonlinear single Compton scattering by an incoming electron described by a wave-packet of Volkov states. We have obtained that the conservation of energy and momentum forbids interference effects among different momentum components of the wave-packet, even if the electron is originally in a superposition of Volkov states. This means that an incoming electron wave-packet can be equivalently described in this respect as a superposition of states or as a statistical mixture. The net effect of having a wave-packet as

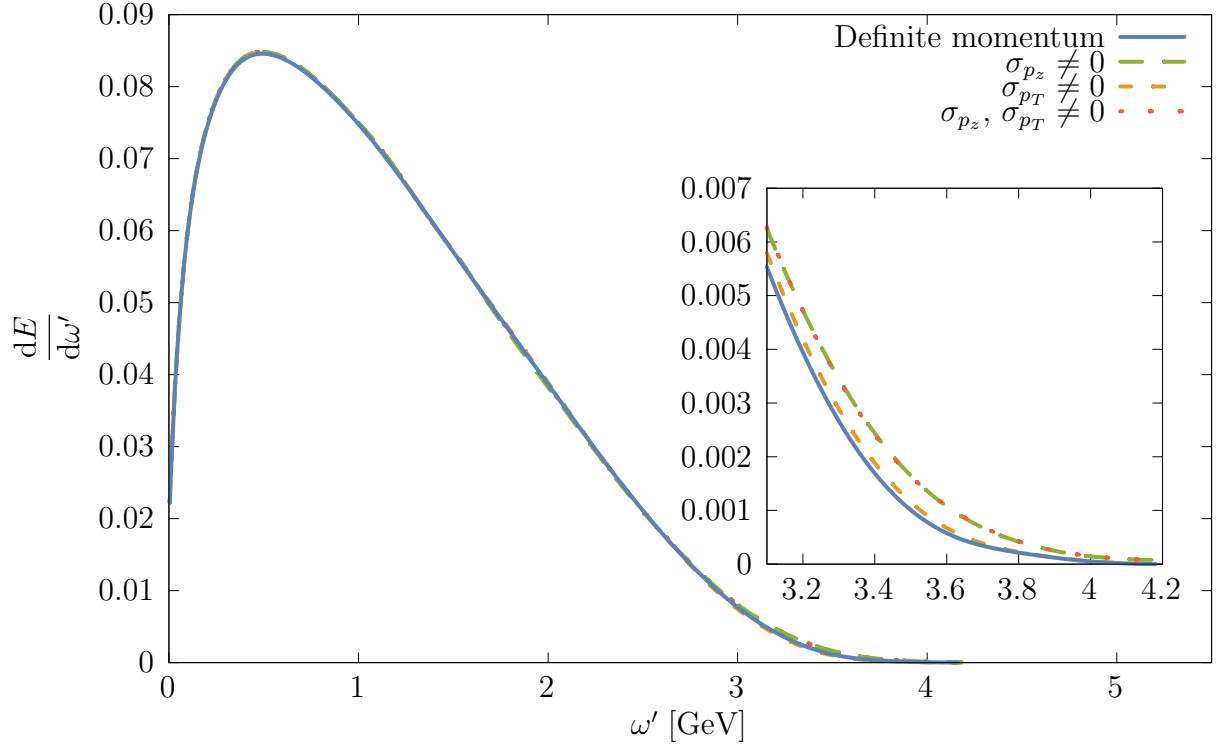


Figure 11. (color online) Distribution of the total emitted energy by an electron in a Volkov state or in a Gaussian wave-packet as a function of the frequency of the emitted photon. All the numerical parameters for this figure are the same as in Fig. 10.

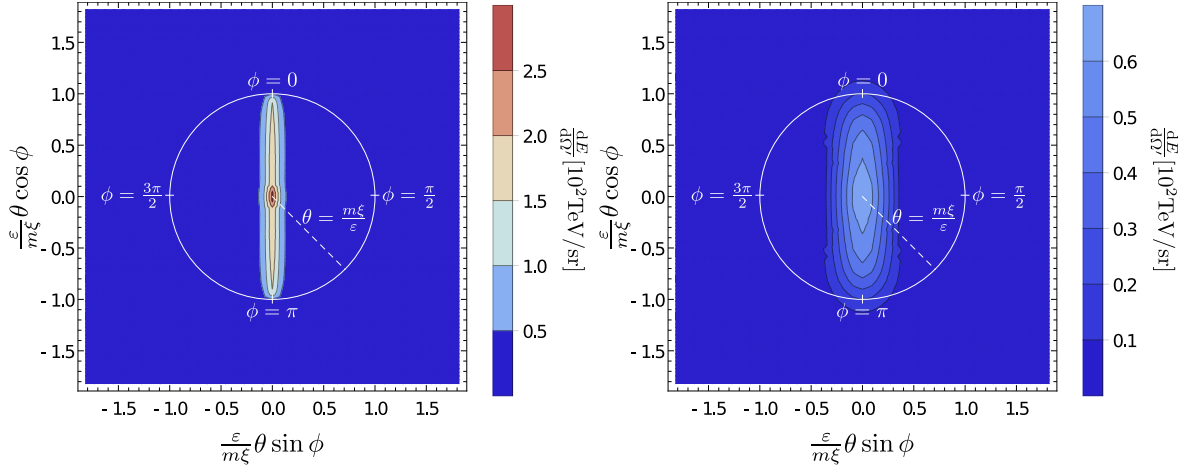


Figure 12. (color online) Angular distribution of the total energy emitted by an electron in a Volkov state (left) or in a Gaussian superposition of them (right) after interacting with a strong laser field. The numerical parameters used here are the same as in Fig. 10.

initial electron state is a lowering and a smoothing of the angular resolved emission spectrum for an electron in a state with definite momentum; this effect tends to be more pronounced than the non-monochromaticity of the laser pulse (at comparable relative uncertainties in the electron and in the laser-photon energy). Furthermore, for realistic values of the properties of the electron wave-packet as compared with those available experimentally for electron beams, the transverse momentum spread, even if orders of magnitude smaller than the longitudinal one, dominates the alterations on the structures and on the shape of the emission spectrum at a fixed observation direction. We have observed that a broadening of the angular emission region takes also place in the case of an electron wave-packet with respect to the case of a monoenergetic electron. However, by integrating the spectra over the observation directions, their dependence on the spreading of the initial wave packet is strongly suppressed.

-
- [1] J. D. Jackson, *Classical Electrodynamics*, (Wiley, New York, 1999).
 - [2] M. E. Peskin and D. V. Schroeder, *Introduction to Quantum Field Theory*, (Addison-Wesley, Reading, 1995).
 - [3] V. B. Berestetskii, E. M. Lifshitz, and L. P. Pitaevskij, *Quantum Electrodynamics*, (Elsevier Butterworth-Heinemann, Oxford, 1982).
 - [4] V. I. Ritus, J. Russ. Laser Res. **6**, 497 (1985).
 - [5] A. Di Piazza, C. Müller, K. Z. Hatsagortsyan, and C. H. Keitel, Rev. Mod. Phys. **84**, 1177 (2012).
 - [6] F. Ehlotzky, K. Krajewska, and J. Z. Kamiński, Rep. Prog. Phys. **72**, 046401 (2009).
 - [7] F. Sauter, Z. Phys. **69**, 742 (1931).
 - [8] H. W. Heisenberg and H. Euler, Z. Phys. **98**, 714 (1936).
 - [9] J. Schwinger, Phys. Rev. **82**, 664 (1951).
 - [10] L. S. Brown and T. W. B. Kibble, Phys. Rev. **133**, A705 (1964).
 - [11] I. I. Goldman, Sov. Phys. JETP **46**, 1412 (1964).
 - [12] A. I. Nikishov and V. I. Ritus, Sov. Phys. JETP **19**, 529 (1964).
 - [13] D. Y. Ivanov, G. L. Kotkin, and V. G. Serbo, Eur. Phys. J. C **36**, 127 (2004).
 - [14] M. Boca and V. Florescu, Phys. Rev. A **80**, 053403 (2009).
 - [15] C. Harvey, T. Heinzl, and A. Ilderton, Phys. Rev. A **79**, 063407 (2009).

- [16] F. Mackenroth, A. Di Piazza, and C. H. Keitel, Phys. Rev. Lett. **105**, 063903 (2010).
- [17] M. Boca and V. Florescu, Eur. Phys. J. D **61**, 449 (2011).
- [18] F. Mackenroth and A. Di Piazza, Phys. Rev. A **83**, 032106 (2011).
- [19] D. Seipt and B. Kämpfer, Phys. Rev. A **83**, 022101 (2011).
- [20] K. Krajewska and J. Z. Kamiński, Phys. Rev. A **85**, 062102 (2012).
- [21] M. Boca, V. Dinu, and V. Florescu, Phys. Rev. A **86**, 013414 (2012).
- [22] M. Boca, V. Dinu, and V. Florescu, Nucl. Instrum. Meth. B **279**, 12 (2012).
- [23] T. N. Wistisen, Phys. Rev. D **90** (2014) 125008.
- [24] D. Seipt, S. G. Rykovanov, A. Surzhykov, and S. Fritzsche, Phys. Rev. A **91**, 033402 (2015).
- [25] K. Krajewska, F. Cajiao Vlez, and J. Z. Kamiński, Phys. Rev. A **91**, 062106 (2015).
- [26] J. Peatross, C. Müller, K. Z. Hatsagortsyan, and C. H. Keitel, Phys. Rev. Lett. **100**, 153601 (2008).
- [27] C. Pellegrini, A. Marinelli, and S. Reiche, Rev. Mod. Phys. **88**, 015006 (2016).
- [28] W. H. Furry, Phys. Rev. **81**, 115 (1951).
- [29] J. P. Corson, J. Peatross, C. Müller, and K. Z. Hatsagortsyan, Phys. Rev. A **84**, 053831 (2011).
- [30] J. P. Corson and J. Peatross, Phys. Rev. A **84**, 053832 (2011).
- [31] D. Strickland and G. Mourou, Opt. Commun. **56**, 219 (1985).
- [32] A. Piskarskas, A. Stabinis, and A. Yankauskas, Phys. Usp. **29**, 869 (1986).
- [33] <http://www.clf.rl.ac.uk/Facilities/Vulcan/12248.aspx>.
- [34] <http://www.clf.stfc.ac.uk/CLF/Facilities/Astra/12254.aspx>.
- [35] <http://cuos.engin.umich.edu/researchgroups/hfs/facilities/hercules-petawatt-laser/>.
- [36] <http://loasis.lbl.gov/>.
- [37] <http://www.eli-laser.eu/>.
- [38] <http://www.hiperlaser.org/>.
- [39] http://cilexsaclay.fr/Phoce/Vie_des_labos/Ast/ast_technique.php?id_ast=9.
- [40] <http://www.xcels.iapras.ru/>.
- [41] V. Malka, J. Faure, Y. A. Gauduel, E. Lefebvre, A. Rousse, and K. T. Phuoc, Nat. Phys. **4**, 447 (2008).

- [42] W. P. Leemans, A. J. Gonsalves, H.-S. Mao, K. Nakamura, C. Benedetti, C. B. Schroeder, Cs. Tóth, J. Daniels, D. E. Mittelberger, S. S. Bulanov, J.-L. Vay, and E. Esarey, Phys. Rev. Lett. **113**, 245002 (2014).
- [43] L. D. Landau and E. M. Lifshitz, *The Classical Theory of Fields*, (Elsevier, Oxford, 2013).
- [44] A. Di Piazza, Phys. Rev. Lett. **113**, 040402 (2014).
- [45] L. N. G. Filon, Proc. R. Soc. Edinb. **49**, 38 (1930).
- [46] A. Iserles and S.P. Nørsett, Proc. R. Soc. A **461**, 1383 (2005).
- [47] D. Volkov, Z. Phys. **94**, 250 (1935).
- [48] F. Mackenroth, *Quantum Radiation in Ultra-Intense Laser Pulses*, (Springer, Heidelberg, 2014).
- [49] P. Baum, Chem. Phys. **423**, 55 (2013).